A model for the propagation of nonlinear surface waves over viscous muds

James M. Kaihatu [a],*, Alexandru Sheremet [b], K. Todd Holland [c]

[a] *Zachry Department of Civil Engineering, Texas A&M University, College Station, TX 77843-3136, United States*
[b] *Department of Civil Engineering, University of Florida, Gainesville, FL 32611-6590, United States*
[c] *Marine Geosciences Division Code 7440.3, Naval Research Laboratory, Stennis Space Center, MS 39529-5004, United States*

Abstract

The effect of a thin viscous fluid–mud layer on nearshore nonlinear wave–wave interactions is studied using a parabolic frequency-domain nonlinear wave model, modified to incorporate a bottom dissipation mechanism based on a viscous boundary layer approach. The boundary-layer formulation allows for explicit calculation of the mud-induced wave damping rate. The model performed well in tests based on laboratory data. Numerical tests show that damping of high frequency waves occurs, mediated by "difference" nonlinear interactions. Simulations of 2-dimensional wave propagation over a mud "patch" of finite extent show that the wave dissipation causes significant downwave diffraction effects.

1. Introduction

The propagation of ocean surface waves has been studied intensively in the last few decades, particularly as numerical models of wave propagation over varying bathymetry have become sufficiently skillful for use in operational forecasting, engineering studies, etc. Both phase-resolving models via the mild-slope (e.g. Berkhoff, 1972) or Boussinesq (e.g. Peregrine, 1967) equations, and phase-averaged models (e.g. Booij et al., 1999), have been extensively validated for cases in which the bottom composition is not a significant concern to the propagation characteristics (sandy beaches). Wave–bottom frictional effects are typically of secondary importance in sandy environments. On spatial scales typical of surf zones on sandy beaches, wave breaking tends to overwhelm bottom friction dissipation rates. Over larger scales (100-km wide North Carolina shelf), swell energy loss rates of 50–75% have been observed, attributed to the interaction of waves with bottom ripples (Ardhuin et al., 2002; Ardhuin et al., 2003).

By comparison, the strength of dissipation processes specific to wave propagation in fine-grained, cohesive sedimentary environments is well known. Extreme dissipation rates have

been routinely reported: 80% wave energy loss over only 2.6 wavelengths (Gade, 1958, laboratory experiments); more than 90% energy loss across the 20-km wide shallow mudflats (Wells and Coleman, 1981, off the coast of Surinam); 95% incident energy loss across 1.1 km-wide mudbanks (Mathew, 1992, off the coast of India), and so on.

Theoretical formulations of bed-induced wave dissipation are based on the assumption that wave motion reaches the bottom and interacts directly with bed sediments. The approaches typically focus on a single (dominant) physical mechanism, defined by the bed state and composition. A number of physical mechanisms for wave dissipation over muddy seabeds have been proposed over time, based on different models of sediment rheology. The diversity of mud states and corresponding beds include poro-elastic solids (Yamamoto et al., 1978; Yamamoto and Takahashi, 1985), viscous Newtonian fluids (Dalrymple and Liu, 1978; Ng, 2000), Bingham fluids (Mei and Liu, 1987), generalized Voight solids (Macpherson, 1980; Hsiao and Shemdin, 1980; Jiang and Mehta, 1995, 1996), and non-Newtonian fluids (Chou et al., 1993; Foda et al., 1993). With the exception of fluidization processes (Foda et al., 1993; DeWit, 1995), these models focus on a single, well-defined mud phase. Although the models predict greatly differing damping effects (Lee, 1995), each may be applicable in some situations (Mei and Liu, 1987).

* Corresponding author. Tel.: +1 979 862 3511.
  E-mail address: jkaihatu@civil.tamu.edu (J.M. Kaihatu).

All the above mechanisms require direct interaction between the wave motion and sediment bed, and thus are essentially *long-wave* dissipation mechanisms. On time/spatial scales comparable to those of wave evolution on a sandy beach ($10^2 T$ or $10^2 \lambda$, with T and λ characteristic wave length and period), direct wave–bed interaction is arguably the dominant dissipation mechanism outside the surf zone. However, many important cohesive sediment coasts, (e.g. Louisiana and Mississippi Bights, USA), exhibit morphological characteristics which allow wave evolution and dissipation on much larger scales. For example, on the inner shelf fronting Atchafalaya (Louisiana, USA), the 10-m isobath is in some places approximately 50 km offshore. Mediated, *indirect* wave-sediment energy exchange processes, typically also second order in magnitude, can become important over such scales. Examples are *short-wave* dissipation, and processes at the interface between a fluid–mud layer and the upper column, such as surface–interface wave interactions (Foda, 1989; Hill and Foda, 1998; Jamali et al., 2003), or Kelvin–Helmholtz/Holmboe-type lutocline instabilities (e.g. Mehta and Srinivas, 1993).

A series of recent field experiments (Sheremet and Stone, 2003; Sheremet et al., 2005) on the Atchafalaya shelf have raised questions about the possible role of surface wave–wave interactions in mediating short wave dissipation in cohesive sedimentary environments. The observations showed unexpected short-wave damping in areas with cohesive bed sediments, in contrast to normal (negligible) short-wave damping over areas with sandy bottoms. Sediment monitoring devices subsequently deployed at the same muddy site showed that strong spectrum-wide wave damping coincided with formation of a fluid–mud layer with sediment concentrations of over 10 kg/m^2.

Nonlinear wave–wave interaction processes should be important over a 20-km shallow (15–20 m depth) muddy shelf. On a typical sandy beach (slope $\approx$ 1%) near-resonant 3-wave interactions are known to cause significant energy transfers over a few wavelengths (Freilich and Guza, 1984; Elgar and Guza, 1985; Agnon et al., 1993; Kaihatu and Kirby, 1995; Agnon and Sheremet, 1997, 2000; Herbers and Burton, 1997 and many others). Strong phase correlations build up between spectral components, and the wave field is no longer Gaussian. However, the role of wave nonlinearity in the evolution of wave spectra in environments characterized by strong (frequency dependent) damping is not well understood. Jiang and Zhao (1989) and Jiang et al. (1990) treated the problem of solitary and cnoidal wave propagation (respectively) over fluid–mud seabeds, using several mud layers of different viscosities to enact the damping and seeking analytical closed-form solutions. Sheremet et al. (2005) incorporated the mud dissipation model of Jiang and Mehta (1995) into the nonlinear 1D triad shoaling model of Agnon et al. (1993) and tested the hypothesis of Sheremet and Stone (2003) concerning the dampening of high frequency waves. Their numerical simulations based on nonlinear wave propagation models suggest that nonlinear energy transfer within the wave spectrum may be important, perhaps providing the coupling between the short- and long-wave spectral bands, allowing energy to flow toward long waves, where it can be efficiently dissipated via direct wave–bottom interaction.

In this study we incorporate a mud-induced energy dampening mechanism into a phase-resolving nonlinear (one-dimensional and parabolic two-dimensional) frequency domain model for surface waves. One of the attractions of the phase-resolving approach is the direct correspondence between properties of the model realizations and data from various remote sensing platforms (e.g. interferometric synthetic aperture radar, surface-mapping lidar, video). This offers great potential for data assimilation and inverse modeling to deduce aspects of the bottom topography and sediment heterogeneity over a large area. We first compare the resulting model to data from a laboratory experiment, then demonstrate some interesting properties of the model in one- and two-dimensional scenarios.

The model developed here describes mud-induced surface wave dissipation and nonlinear processes but does not account for the complexities of the coupling between sediment and wave states (feedback between waves and fluid mud layer). However, our focus at the present is on a wave model which can be applied in general situations of wave propagation over muddy bottoms, rather than a detailed investigation of the processes at the interface. This is not unlike many previous studies detailing the representation of wave breaking dissipation into a surface wave model by the inclusion of an additional term (e.g. Kirby and Dalrymple, 1986).

2. Viscous dissipation mechanism of Ng (2000)

The dispersion relation for a linear system can be generically written as:

$$\Omega(\omega, K, h) = 0, \tag{1}$$

which relates wavenumber K to water depth h and frequency ω (Whitham, 1974). For linear dissipative systems the solutions K of the dispersion relation (1) are complex, and are typically found by a laborious search in the complex plane (e.g. the complex secant method used by Dalrymple and Liu, 1978). The accuracy of the calculation of the complex roots is also an important concern, particularly when incorporating the algorithms into a numerical model with nonlinear terms which are sensitive to the nature and degree of dissipation, as has been observed with surf zone breaking (Kirby and Kaihatu, 1996). Numerical applications of wave modeling require an efficient and robust approach for calculating these roots, particularly in the case of nonlinear models which spend significant computational resources on the calculation of nonlinear terms. Here, we investigate the simplified approach developed by Ng (2000), which has the potential to approximate the physics of mud-induced dissipation well enough to allow reliable calculation of the dissipative modes K.

Laboratory observations by Gade (1958) and numerical simulations based on the model developed by Dalrymple and Liu (1978) suggest that mud-induced wave dissipation is maximized when the mud layer is approximately 1.5 times the boundary layer depth in the viscous fluid, thus setting up the requisite scales for a boundary layer solution. The idea was pursued by Ng (2000), who formulated the viscous dissipation

mechanism as a boundary layer reduction of the Dalrymple and Liu two-layer fluid model. Assuming that the depth of the mud layer is comparable to the mud layer's Stokes boundary layer thickness implies that

$$ka \simeq kd_m \simeq k\delta_m \ll 1, \tag{2}$$

where $k=Re(K)$, a is the wave amplitude, d_m the depth of the mud layer, and $\delta = \sqrt{2v/\delta}$ is the Stokes boundary layer thickness, where v is the kinematic viscosity and σ is the angular frequency of the wave. The subscript m denotes mud. As a result of this scaling, the wavenumber of a dissipative mode can be written as

$$K = k_1 + k_2, \text{ with } |k_1| \gg |k_2|, \tag{3}$$

where the leading order term k_1 is real and satisfies the non-dissipative dispersion relation

$$\omega^2 = gk_1 \tanh k_1 h, \tag{4}$$

written in the absence of any fluid–mud layer. The second order correction k_2 is complex and incorporates the effect of the fluid mud. For k_2, Ng (2000) obtains

$$k_2 = -\frac{Bk_1}{\sinh k_1 h \cosh k_1 h + k_1 h} \tag{5}$$

The imaginary part of the wavenumber k_2 is the damping rate:

$$D = Im(k_2) = -\frac{Im(B)k_1}{\sinh k_1 h \cosh k_1 h k_1 h} \tag{6}$$

where B is a complex coefficient

$$Re(B) = \frac{k_1 \delta m(B_1 - B_2)}{2B_3} + \gamma k_1 dm, \tag{7}$$

$$Im(B) = \frac{k_1 \delta m(B_1 + B_2)}{2B_3}, \tag{8}$$

with

$$
\begin{aligned}
B_1 = {}& \gamma(-2\gamma^2 + 2\gamma - 1 - \zeta^2)\sinh \tilde{d} \, \cosh \tilde{d} - \gamma^2 \zeta \\
& \times (\cosh^2 \tilde{d} + \sinh^2 \tilde{d}) - (\gamma^2 - 1)^2 \zeta \\
& \times (\cosh^2 \tilde{d} \cos^2 \tilde{d} + \sinh^2 \tilde{d} \sin^2 \tilde{d}) - 2\gamma(1 - \gamma) \\
& \times (\zeta \cosh \tilde{d} + \gamma \sinh \tilde{d})\cos \tilde{d},
\end{aligned}
\tag{9}
$$

$$
\begin{aligned}
B_2 = {}& \gamma(-2\gamma^2 + 2\gamma - 1 + \zeta^2)\sin \tilde{d} \cos \tilde{d} - 2\gamma(1 - \gamma) \\
& \times (\zeta \sinh \tilde{d} + \gamma \cosh \tilde{d})\sin \tilde{d},
\end{aligned}
\tag{10}
$$

$$B_3 = (\zeta \cosh \tilde{d} + \gamma \sinh \tilde{d})^2 \cos^2 \tilde{d} + (\zeta \sinh \tilde{d} + \gamma \cosh \tilde{d})^2 \sin^2 \tilde{d}. \tag{11}$$

The solutions ((4)–(5)) is a function of nondimensional parameters: $\gamma = \rho_w/\rho_m$, where ρ is the density; $\zeta = \delta_m/\delta_w = (v_m/v_w)^{1/2}$; and $\tilde{d} = d/\delta_m$. The subscript w refers to water. The real part of the second order correction k_2 represents the modification to the wavelength due to the viscous mud. The total real part of the wavenumber k is determined as:

$$k = k_1 + Re(k_2) = k_1 - \frac{Re(B)k_1}{\sinh k_1 h \cosh k_1 h + k_1 h} \tag{12}$$

The solution ((4)–(5)) is remarkable in that mud effects are explicitly expressed in terms of the first order, nondissipative, real, wavenumber k_1.

The characteristics of the dissipation (6) had been discussed by Ng (2000, see Figs. 2 and 3); however the effect of a thin viscous layer of mud on the wavenumber k was not similarly explored by Ng (2000). This companion effect of mud on the real part k of the wavenumber is important for nonlinear effects in wave spectra since the wavenumbers determine the amount of detuning away from resonance, and thus directly affect energy transfer within the wave spectrum. Fig. 1 shows the effect of the mud on real part of the wavenumber for two different values of ζ ($\zeta = 10$) and $\zeta = 100$), where the density ratio $\gamma = 0.9$; the boundary layer scale δ_m was kept constant while the mud layer depth d_m was varied with the dimensionless depth $\tilde{d}$. Clearly the increasing mud layer causes a decrease in the wavenumber k relative to that with no mud. The convention typically used in theories of wave propagation over mud has the mud layer adding to the total water depth; the wave experiences an increase in water depth with the addition of the mud layer, and the resulting decrease in wavenumber is similar to an inverse shoaling effect. The degree to which the wavenumber decreases is dependent on the mud properties. A comparison to a similar figure shown in Dalrymple and Liu (1978; Fig. 3) reveals that the present theory has a smaller rate of wavenumber decrease to increase of $\tilde{d}$. This is sensible since the validity of the boundary layer approximation in Ng (2000) decreases with increasing $\tilde{d}$.

Fig. 2 shows the variation of (6), normalized by the maximum dissipation D_{max} for each parameter set, with kh. This normalization is done to help visualize the shape of the frequency dependence and reveal the similarity across mud parameter sets; the value of D_{max} for these parameters actually varies over three orders of magnitude. For this analysis, the water depth $h=1$ m. We use $\gamma = (0.5, 0.9)$ and $\zeta = (10, 100)$. For $\zeta = 10$ we set $d_m = 0.02$ m, and for $\zeta = 100$ we use $d_m = 0.2$ m. This allows $\tilde{d}$ to have the same values over the range of kh for all mud parameters used. Despite the differences in mud parameters, the curves have a very similar shape and maxima which are located near $kh \sim 0.88$. All curves are characterized by a rapid rise from minimal dissipation for $kh < 0.88$ and a relatively slow fall to zero damping with $kh > 0.88$. This is because waves in very shallow water (low kh) will have mud boundary layer thicknesses δ_m which are greater than the depth of the mud layer (low $\tilde{d}$). Relatively little damping thus occurs. Conversely, waves in deeper water (high kh) will
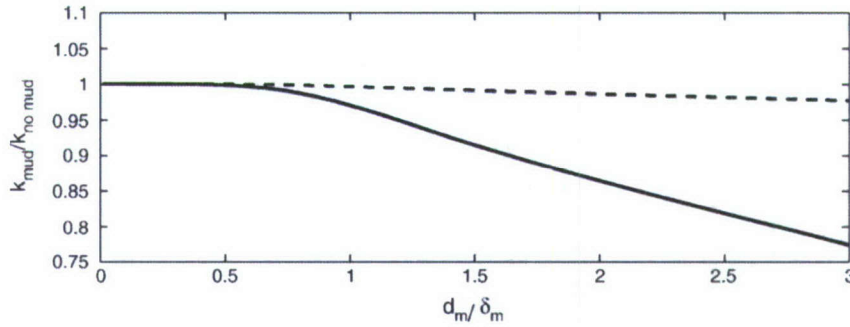
Fig. 1. Effect of viscous mud layer on wavenumber. Solid line: $\zeta = 100$, $\gamma = 0.9$. Dashed line: $\zeta = 10$, $\gamma = 0.9$.

not be as influenced by the bottom, and thus also experience little damping. The damping appears to be at least 33% of the maximum value in the range $0.1 \leq kh \leq 2.4$, encompassing the upper end of the shallow water range ($kh \leq \pi/10$) and most of the intermediate depth range ($\pi/10 \leq kh \leq \pi$). We note here that different values of d_m will lead to a different range of $\tilde{d}$ over the range of kh considered. This will in turn lead to different values of kh at which the dissipation is maximum.

3. Numerical model for nonlinear wave transformation over a viscous mud layer

We now turn our attention toward the implementation of this mechanism into a wave model. This is done as a superposition of an added dissipation effect into the model, as previously noted.

We use the nonlinear model of Kaihatu and Kirby (1995), which is a parabolic frequency-domain mild-slope equation model with second-order nonlinear wave–wave interactions. The free surface η is assumed to be expressible as:

$$\eta(x, y, t) = \sum_{n=1}^{N} \frac{A_n}{2} e^{i\left(\int k_n dx - \omega_n t\right)} + c.c \qquad (13)$$

where A_n is the complex amplitude of the free surface elevation, "c.c." denotes complex conjugate of the term in the square brackets, and k_n is the wavenumber associated with the radian frequency ω_n. With this and the boundary value problem for water waves (extended to second order in wave amplitude a),

Kaihatu and Kirby (1995) derived the following parabolic equation for A_n:

$$2i(kCC_g)_n \frac{\partial A_n}{\partial x} - 2(kCC_g)_n(\bar{k}_n - k_n)A_n + i\frac{\partial(kCC_g)_n}{\partial x}A_n$$

$$+ \frac{\partial}{\partial y}\left([CC_g]_n \frac{\partial A_n}{\partial y}\right) = \frac{1}{4}\left(\sum_{l=1}^{n-1} R_{n,l}A_l A_{n-l}e^{i\int(\bar{k}_l + \bar{k}_{n-l} - \bar{k}_n)dx}\right.$$

$$\left. + 2\sum_{l=1}^{N-n} S_{n,l}A_l^* A_{n+l}e^{i\int(\bar{k}_{n+l} - \bar{k}_l - \bar{k}_n)dx}\right) \qquad (14)$$

where C is the phase velocity, C_g is the group velocity, and R and S are interaction coefficients

$$R_{n,l} = \frac{g}{\omega_l \omega_{n-l}}\left[\omega_n^2 k_l k_{n-l} + (k_l + k_{n-l})(\omega_{n-l}k_l + \omega_l k_{n-l})\omega_n\right]$$

$$- \frac{\omega_n^2}{g}\left(\omega_l^2 + \omega_l \omega_{n-l} + \omega_{n-l}^2\right) \qquad (15)$$

$$S_{n,l} = \frac{g}{\omega_l \omega_{n+l}}\left[\omega_n^2 k_l k_{n+l} + (k_{n+l} - k_l)(\omega_{n+l}k_l + \omega_l k_{n+l})\omega_n\right]$$

$$- \frac{\omega_n^2}{g}\left(\omega_l^2 - \omega_l \omega_{n+l} + \omega_{n+l}^2\right) \qquad (16)$$

The wavenumber $\bar{k}$ is averaged in the y direction, and is a consequence of the parabolic approximation (Radder, 1979), which in practical terms limits the obliquity of the wave with respect to the x axis of the grid. Details of the derivation are presented in Kaihatu and Kirby (1995) and not replicated here. The primary advantage of the model is that the shoaling and
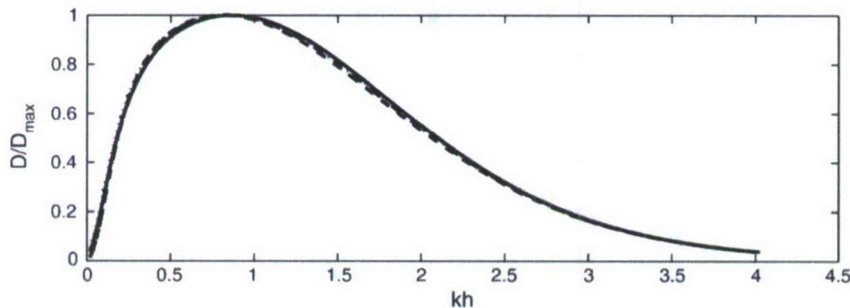

Fig. 2. Dissipation D (normalized by the maximum) as a function of relative water depth kh. Water depth $h = 1$ m. Solid line: $\zeta = 10$, $\gamma = 0.9$, $d_m = 0.02$ m. Dashed line: $\zeta = 100$, $\gamma = 0.9$, $d_m = 0.2$ m. Dotted line: $\zeta = 10$, $\gamma = 0.5$, $d_m = 0.02$ m. Dash-dot line: $\zeta = 100$, $\gamma = 0.5$, $d_m = 0.2$ m.

dispersion are determined by fully-dispersive linear theory, thus overcoming the shallow water limitation of classical Boussinesq type models (e.g. Freilich and Guza 1984; Liu et al., 1985). Since the equation is parabolic, numerical solution is easily undertaken via the Crank–Nicholson method, iterated to center the nonlinear terms between the cross-shore grid points. The process of parabolization reduces the computational effort, but disallows processes which run backward through the domain such as back reflection. Kaihatu and Kirby (1995) showed that (14) compared well to laboratory data. The parabolic model was extended to wide angles of propagation by Kaihatu (2001).

Kaihatu and Kirby (1995) also used a one-dimensional reduction of (14) for shoaling waves, and extended it into the surf zone by the addition of a spectral dissipation term:

$$A_{nx} + \frac{(CC_g)_{nx}}{(2CC_g)_n} A_n + \alpha_n A_n = -\frac{i}{8(kCC_g)_n}$$

$$\times \left[\sum_{l=1}^{n-1} RA_l A_{n-l} e^{i\int (k_l + k_{n-l} - k_n)dx} \right.$$

$$\left. +2 \sum_{l=1}^{N-n} A_l^* A_{n+l} e^{i\int (k_{n+l} - k_l - k_n)dx} \right] \quad (17)$$

where α is the dissipation coefficient due to surf zone dissipation; this term is detailed in Kaihatu and Kirby (1995). Comparisons with data yielded excellent results. A nonlinear correction term was added to the model by Kaihatu (2001), which led to improved wave shape predictions. We do not employ the surf zone dissipation in this study, but reserve it for analysis in a future study. This equation was numerically solved with a fourth-order Runge–Kutta scheme.

Similar to the development of the breaking term implementation in Kirby and Dalrymple (1986), we add the dissipation mechanism of Ng (2000) directly to the equations in a manner consistent with the conservation of energy flux. Thus (14) becomes:

$$2i(kCC_g)_n \frac{\partial A_n}{\partial x} + 2i(kCC_g)_n D_n A_n - 2(kCC_g)_n (\bar{k}_n - k_n) A_n$$

$$+ i \frac{\partial (kCC_g)_n}{\partial x} A_n + \frac{\partial}{\partial y}\left([CC_g]_n \frac{\partial A_n}{\partial y}\right) = \frac{1}{4}$$

$$\times \left(\sum_{l=1}^{n-1} R_{n,l} A_l A_{n-l} e^{i\int (\bar{k}_l + \bar{k}_{n-l} - \bar{k}_n)dx} \right.$$

$$\left. +2 \sum_{l=1}^{N-n} S_{n,l} A_l^* A_{n+l} e^{i\int (\bar{k}_{n+l} - \bar{k}_l - \bar{k}_n)dx} \right) \quad (18)$$

and (17) becomes:

$$A_{nx} + \frac{(CC_g)_{nx}}{(2CC_g)_n} A_n + D_n A_n = -\frac{i}{8(kCC_g)_n}$$

$$\times \left[\sum_{l=1}^{n-1} RA_l A_{n-l} e^{i\int (k_l + k_{n-l} - k_n)dx} \right.$$

$$\left. +2 \sum_{l=1}^{N-n} A_l^* A_{n+l} e^{i\int (k_{n+l} - k_l - k_n)dx} \right] \quad (19)$$

where $D_n = D(\omega_n, k_{1n}, h)$ is as in (6).

4. Model results

This section presents a number of consistency and model data comparison tests performed with the model (18) to ascertain the effect of the mud on wave transformation. As a consistency check, we first compare the model to laboratory data for a simple case of wave propagation over a flat, muddy bottom. After confirming the performance of the model, we then use it to examine the physical nature of nonlinear wave propagation over viscous muds. In particular, we analyze the effect of mud on nonlinear energy transfer, focusing on the attenuation of high frequency energy.

4.1. Comparison with laboratory data

Most of the existing field or laboratory data sets on wave propagation over muddy sea beds (e.g. Gade 1958; Tubman and Suhayda, 1976; Forristall and Reece, 1985; Jiang and Mehta, 1995) focus on linear processes of narrow-spectrum long waves. Their approach is based on the assumption that bottom interaction is significant only for the long waves, which reach deep enough in the water column to interact directly with the bottom. A number of field experiments were conducted recently, dedicated to monitoring nonlinear aspects of wave evolution (e.g. Jaramillo et al., 2006) but as this paper was written the data from these experiments were still being processed. A detailed analysis of the performance of the model in field data tests will be presented elsewhere. Here, we will limit scope of the model–data comparison to some simple consistency checks against laboratory data of De Wit (1995), who investigated the liquefaction of cohesive sediments in a flume under varying conditions of waves and currents.

The flume used to perform the experiments was 40 m long, with a width and depth of 0.8 m. The flume was fitted with a false floor of depth 0.2 m and length 8 m, allowing an overall maximum depth of 1 m. In this area dense mud was emplaced. De Wit (1995) performed tests using several clays; we use his results from Experiment III, in which China clay (kaolinite is a principal mineral component) was used. The clay powder was mixed with 0.5% solution of sodium chloride to a sediment concentration of 275 kg/m³, then allowed to consolidate for 6 days. This resulted in a suspension with a density of about 1300 kg/m³. Its viscosity $v_m = 2.7 \times 10^{-3}$ m²/s. We assumed $v_w = 1.3 \times 10^{-6}$ m²/s.

Two other tests in Experiment III were carried out over this material. The material was then allowed to rest for one day. Test 3 of Experiment III was then conducted. The mud parameters and wave conditions used are shown in Table 1. This experiment was also used to validate a more comprehensive mud dissipation model (Winterwerp et al., 2007).

Table 1
Mud parameters and wave condition: Test 3 of Experiment III of De Wit (1995)

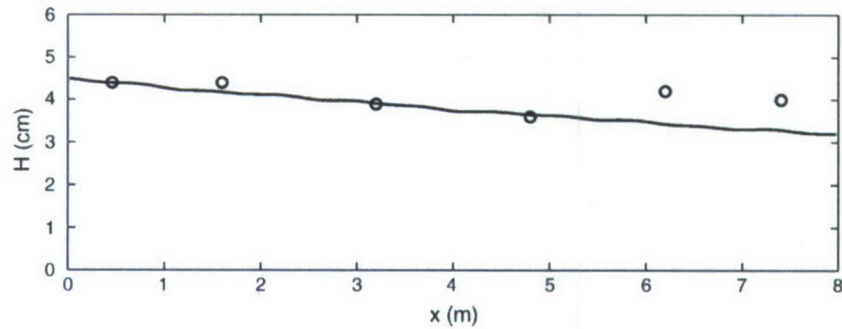| ρ_w (kg/m³)	ρ_m (kg/m³)	d_m (m)	h (m)	H (m)	v_m (m²/s)	T (s)
1000	1300	0.115	0.325	0.045	2.6×10^{-3}	1.5

Fig. 3. Comparison of model to data from De Wit (1995), Test 3 of Experiment III. Solid line: waveheights from model. Circles: measurements.

We used a permanent form solution of (17) without the dissipation terms. This solution consisted of seven harmonics phase-locked to the primary mode with amplitudes spanning six orders of magnitude; details on this solution technique are provided by Kaihatu (2001). The amplitude series comprising this waveform were input into the model and run over the 8 m long mud section. Waveheights were calculated at the gage locations by reconstructing the waveform and determining the distance between crest and trough. The resulting comparison is shown in Fig. 3; agreement is good and on a par with that shown by Winterwerp et al. (2007). This is particularly noteworthy in that the depth of the mud layer is roughly 33% of the water depth, which would appear to violate the thin layer assumption inherent in the formulation of Ng (2000). In fact, the largest of
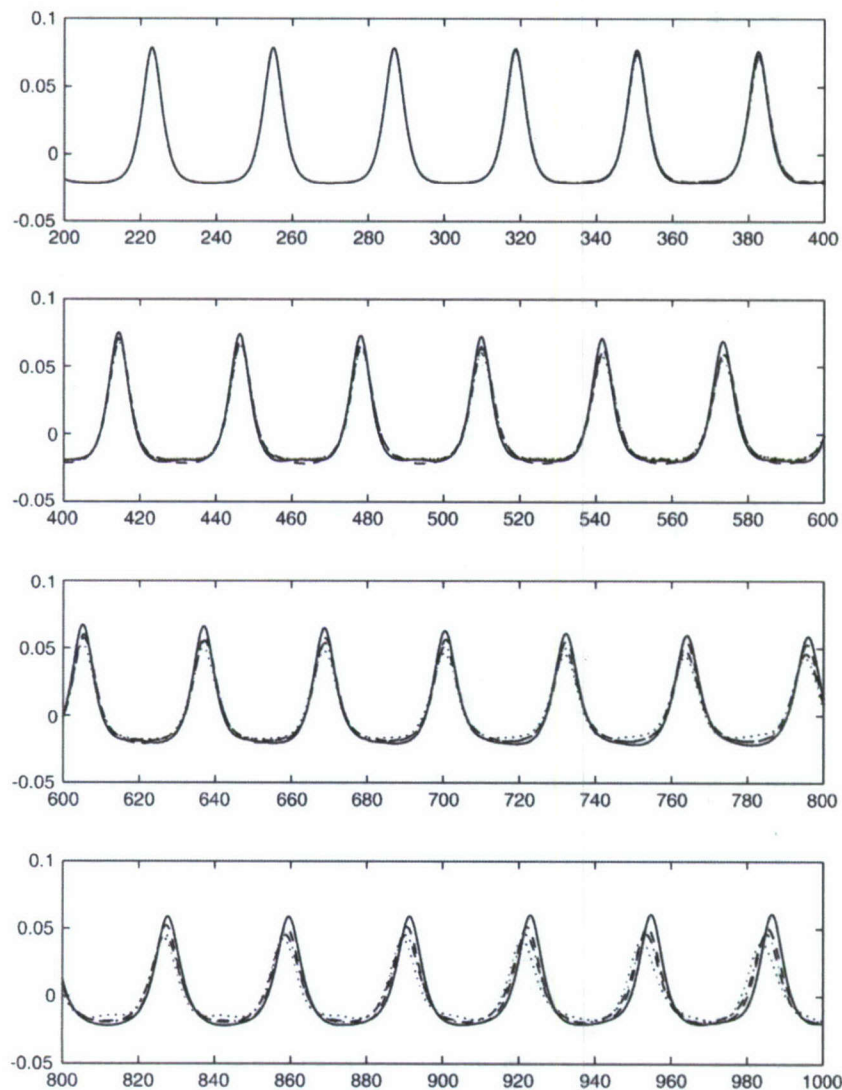

Fig. 4. One-dimensional cnoidal waves over mud patch: $\zeta=10$ case. Solid line: $\gamma=0.25$. Dashed line: $\gamma=0.5$. Dash–dot line: $\gamma=0.75$. Dotted line: $\gamma=0.9$.

the scales (2) used by Ng (2000) is $kd_m=0.3$, which is not very small. However the fact that the model still compared well to data indicates that the scaling assumption is perhaps not that restrictive, at least as far as the damping is concerned. We note here that the sudden increase in measured waveheight near the downwave end of the mud patch was likely caused by wave reflection from the back of the mud pit. Due to the parabolic nature of the model, this effect cannot be simulated. Using linear long wave theory (Dean and Dalrymple, 1991) the expected reflection is estimated to be 10% of the incident wave energy. This slightly overestimates the error between model and measurement beyond $x=5$ m, possibly due to the use of linear long wave theory for its estimation.

4.2. Permanent form shallow water waves over a flat bottom — effects of mud

Similar to the previous test, our next test involves the transformation of waves of permanent form over a flat bottom in which a region of mud has been placed. However, in this test we will investigate the damping of shallow water waves across long transformation distances. Our domain is 1000 m long, with a constant depth of 1 m and a grid resolution $\Delta x=0.025$ m. In actual practice this is far finer than required for an accurate solution, but is used to sharply resolve the free surface η in a post-processing step (via Eq. (13)) once the complex amplitudes A_n are calculated by the model. We define a "mud patch" which extends from $x=300$ m to $x=800$ m. We note here that the length of the domain, the water depth and the extent of the mud patch were chosen to bring forth particular features of the mud dissipation effect on wave–wave interaction, as will be seen. However, these values are comparable to many areas in the world with long shallow shelves and muddy bottoms. For example, the shelf near Marsh Island in Louisiana, USA is extremely flat and less than 2 m in depth over a distance of around 7 km (Sheremet, personal communication). As before, reflection of the wave energy is not considered herein. From linear long wave theory (Dean and Dalrymple, 1991) the expected reflection due to the mud patch is estimated to be less than 5% of the incident energy.
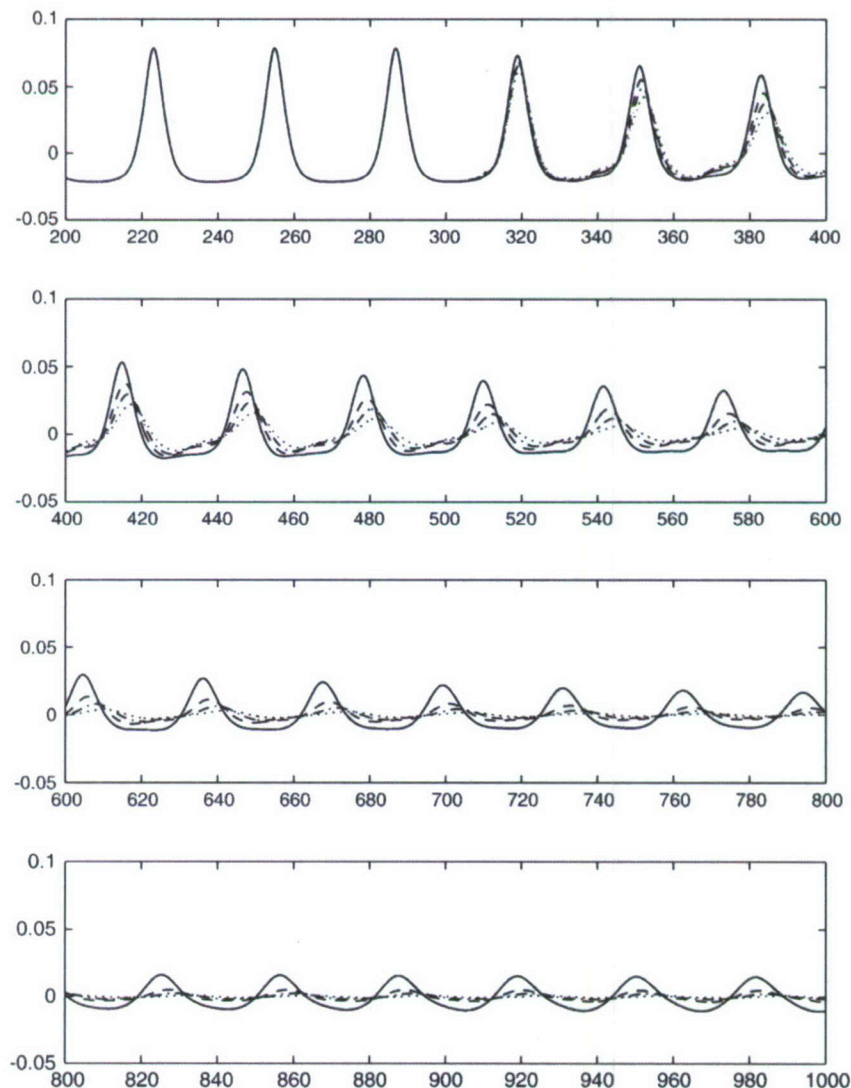

Fig. 5. One-dimensional cnoidal waves over mud patch: $\zeta=100$ case. Solid line: $\gamma=0.25$. Dashed line: $\gamma=0.5$. Dash–dot line: $\gamma=0.75$. Dotted line: $\gamma=0.9$.

We investigate the wave behavior with two different sets of parameters to describe the mud layer. The first uses a depth of mud of 0.02 m and a mud kinematic viscosity $v_m = 1.3 \times 10^{-4}$, leading to $\zeta = 10$ if we assume the kinematic viscosity of water $v_w = 1.3 \times 10^{-6}$. The dimensionless mud depth $\tilde{d} = d_m / \delta_m = 1$. The second case uses $v_m = 1.3 \times 10^{-2}$, making $\zeta = 100$. In order to keep the dimensionless mud depth $\tilde{d} = 1$ we increase the mud layer depth $d_m = 0.2$ m. We will simply refer to them as the $\zeta = 10$ case and the $\zeta = 100$ case. For each case we vary the density ratio $\gamma = (0.25, 0.5, 0.75, 0.9)$, with the most dampening occurring for $\gamma = 0.9$, keeping ζ fixed.

Our shallow water incident wave is a permanent form solution of (17), with a period $T = 10$ s and a height $H = 0.1$ m. With this wave period, we find that $kd_m = 0.04$, which is sufficiently small. The solution is generated via the technique described in Kaihatu (2001) using $N = 15$ frequency components.

Fig. 4 shows free surface elevations for the $\zeta = 10$ case. As expected the greatest amount of dampening was seen when $\gamma = 0.9$. However, it is also interesting that the modification to the wavelength by the presence of mud did not cause significant detuning of the phase locking required to maintain permanent form; the wave retained a mostly-cnoidal shape within and beyond the mud patch even for high γ values.

Fig. 5 shows the case for $\zeta = 100$. The damping is far more dramatic for this case than for $\zeta = 10$; for the $\gamma = 0.9$ case the wave almost disappears entirely. To the extent that the wave shape is discernible at high γ, a somewhat more sinusoidal shape is apparent.

The amplitudes of the frequency components of the wavefield are shown in Fig. 6 for both the $\zeta = 10$ and $\zeta = 100$ cases, for all values of γ used. For both cases, both the initial condition at $x = 0$ and the resulting amplitudes at the end of the mud patch ($x = 800$ m) are shown. The monotonic decrease in amplitude with increasing frequency is apparent for the $\zeta = 10$ case at $x = 800$ m, and is also reflected in the retention of the cnoidal-like shape of the wavefield (Fig. 4). In contrast, the $\zeta = 100$ case shows a distinct non-monotonicity with frequency; the fourth harmonic of the wave ($f = 0.4$ Hz) displays the greatest amount of dissipation (relative to the initial amplitude) from the mud patch in the range $f < 1$ Hz ($kh \sim \pi$). At $f < 0.4$ Hz, $kh \sim 0.89$, which is close to the point of maximum dissipation displayed in Fig. 2.
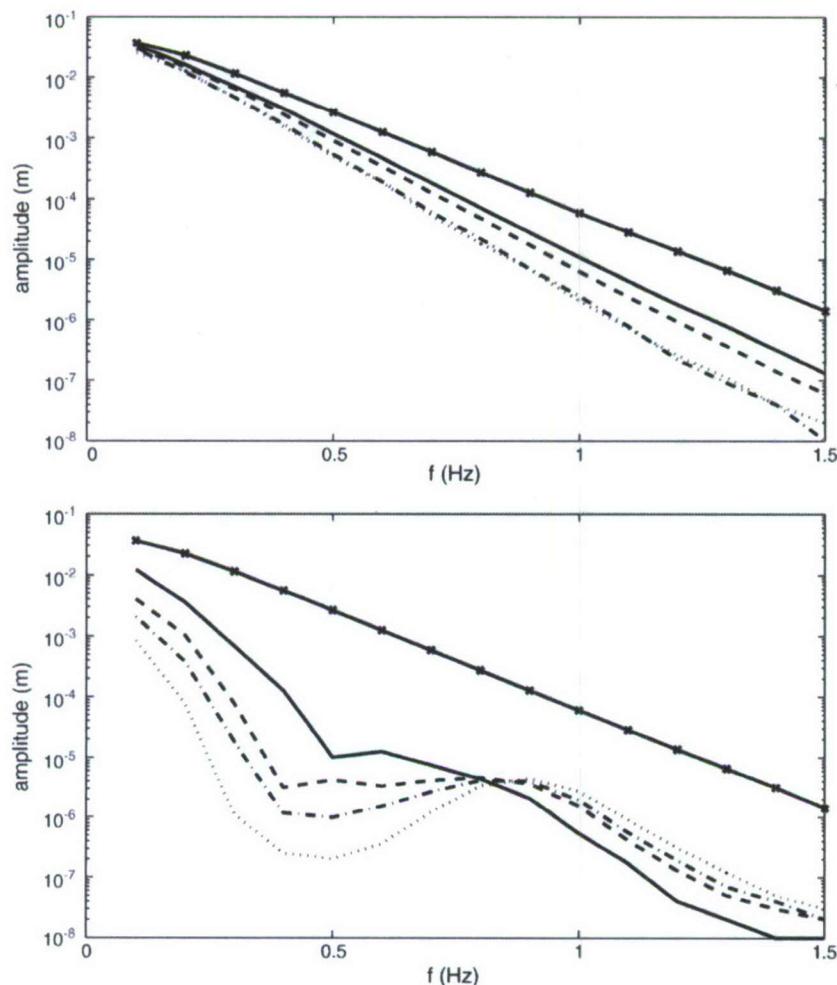

Fig. 6. One-dimensional cnoidal waves over mud patch: amplitudes of wavefield at $x = 0$ (dash–x line) and at downwave end of mud patch ($x = 800$ m). Solid line: $\gamma = 0.25$. Dashed line: $\gamma = 0.5$. Dash–dot line: $\gamma = 0.75$. Dotted line: $\gamma = 0.9$. Top: $\zeta = 10$. Bottom: $\zeta = 100$.

Interestingly, it is also evident that there is a significant loss of amplitude at the high frequencies over the mud patch. The relative depth kh is around 9 at $f=1.5$ Hz, far beyond the kinematical deep water limit. It is thus likely that subharmonic interaction with the lower, actively-damped frequencies is causing this reduction in amplitude, as shown by Sheremet et al. (2005) for the case of a wave group. To investigate this we re-run the model for the case of $\gamma=0.9$, using both $\zeta=10$ and $\zeta=100$. The first run is linear, with the nonlinearity in (17) deactivated. The second run reduces the nonlinear interactions by deactivating the subharmonic interactions (the first summation on the right side of Eq. (17)). If the subharmonic interactions are in fact causing the depletion of energy in frequencies beyond the deep water limit, we would expect to see similar amplitudes between the linear and reduced nonlinear models.

Fig. 7 compares the resulting evolution characteristics between the full model (17), the linearized model, and the reduced nonlinear model (with subharmonic evolution deactivated), for $\gamma=0.9$ and both $\zeta=10$ and $\zeta=100$. There is a close correspondence between the linear and the reduced nonlinear model at the downwave side of the mud patch, indicating that the (deactivated) subharmonic interactions are responsible for

the reduction in amplitudes at high frequencies, as seen in the results of the full model. The high frequency amplitudes of the reduced nonlinear model are elevated slightly over those of the linear model due to superharmonic interactions moving energy from the low frequencies.

5. Two dimensional wave propagation over mud

Our next set of simulations involves the propagation of a two dimensional wave field over a small patch of mud, with emphasis placed on the refraction and diffraction patterns apparent over, and in the lee of, the patch.

We use a two-dimensional domain that is 2000 m in the propagation direction by 600 m in the longshore direction, and use closed lateral boundaries. The extent in the propagation direction should allow enough distance to display significant diffraction effects in the lee of the mud patch. We use the $T=10$ s wave used previously for the one-dimensional case as our initial condition. The bathymetry is a constant depth ($h=1$ m) as before. Into this domain we add a region of mud ($200 \leq x_{mud} \leq 500$ m, 150 m $\leq y_{mud} \leq 450$ m) with $d_m=0.2$ m, $\gamma=0.9$ and $\zeta=100$. The grid resolution used is $\Delta x=0.3$ m and
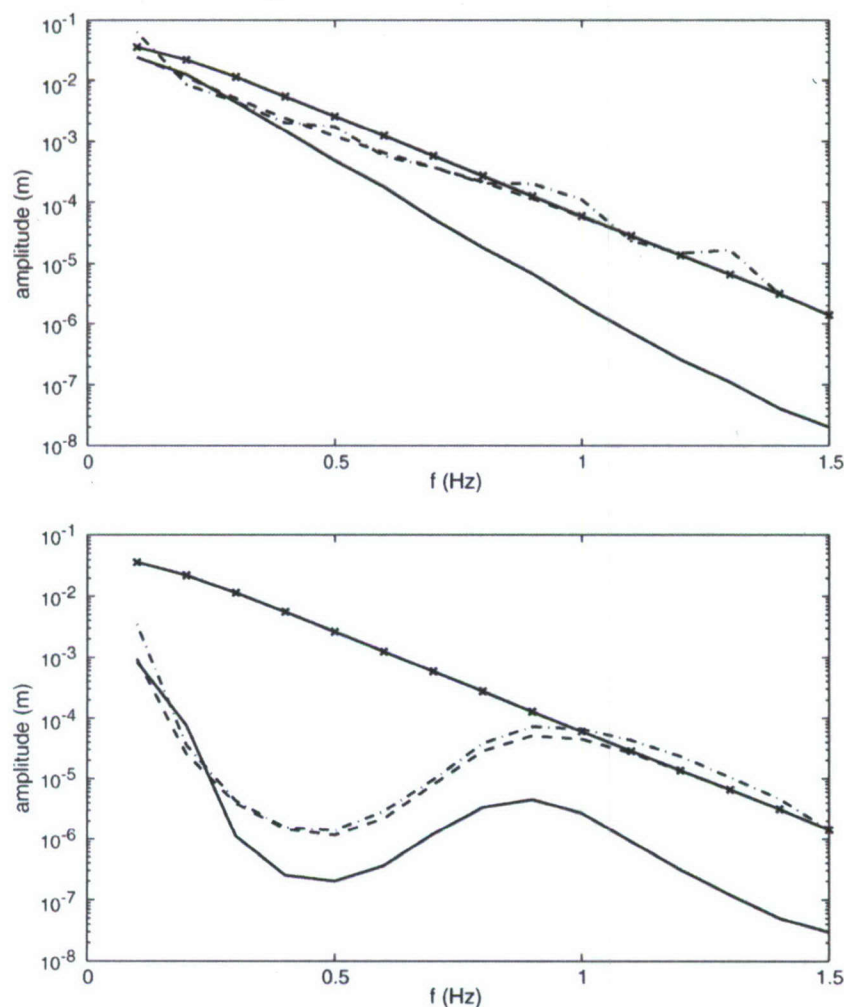

Fig. 7. One-dimensional cnoidal waves over mud patch with $\gamma=0.9$: amplitudes of wavefield at $x=0$ (dash–x line) and at downwave end of mud patch ($x=800$ m). Solid line: Eq. (11). Dashed line: Linear model. Dash-dot line: Eq. (11) with only superharmonic interactions. Top: $\zeta=10$. Bottom: $\zeta=100$.
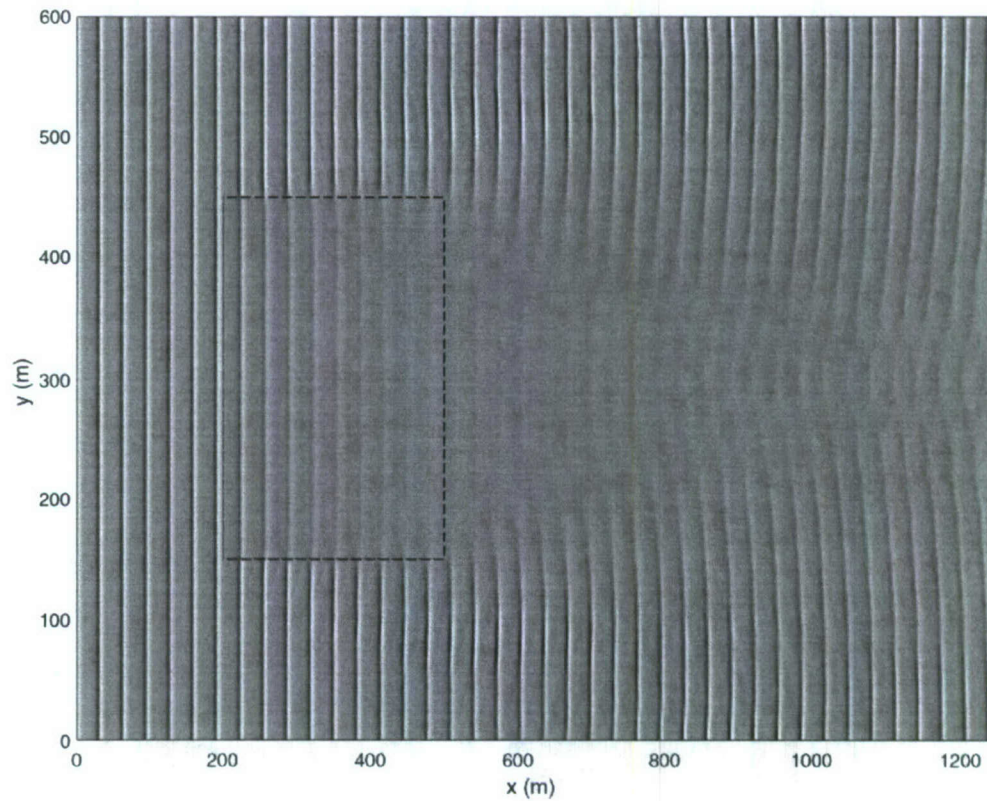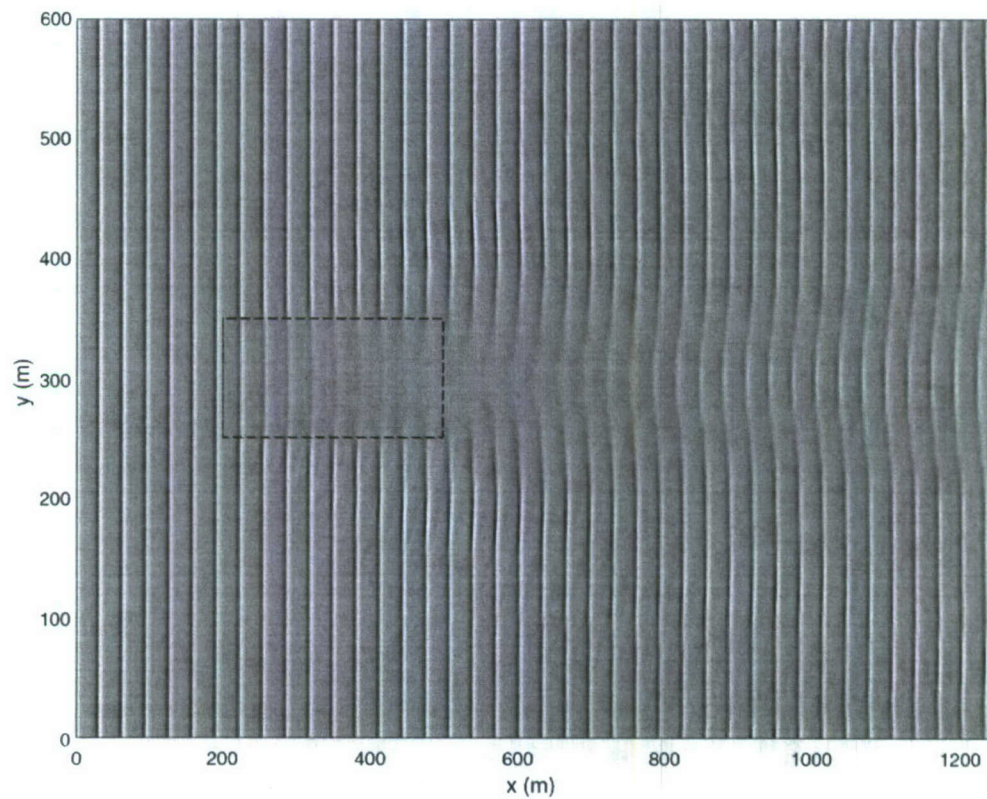
Fig. 8. Cnoidal waves propagating over two-dimensional mud patch: overhead view of free surface elevation (crests are in light streaks). Mud patch boundary shown in dashed lines. Mud parameters: $d_m=0.2\ m$, $\gamma=0.9$, $\zeta=100$.

Fig. 9. Cnoidal waves propagating over two-dimensional mud patch: overhead view of free surface elevation (crests are in light streaks). Mud patch boundary shown in dashed lines, and is reduced in longshore extent. Mud parameters: $d_m=0.2\ m$, $\gamma=0.9$, $\zeta=100$.

$\Delta y=0.6$ m; again this is far finer than required for accurate solution but serves to help sharpen the depiction of the free surface from the complex amplitudes. (We note here that our resolution in the propagation direction Δx is decreased relative to that of the one-dimensional case due to the extra memory requirements incurred by the expansion to two horizontal dimensions.)

The result is shown in Fig. 8. There is a very strong attenuation of the wave elevation through the mud patch and a very long shadow zone in the lee of the patch. Additionally, the wave crests inside the mud patch appear rounder and less sharp than those outside the patch, likely due to the preferential dampening of the higher frequency components of the wave. As the waves propagate past the mud patch, wave diffraction moves energy into the shadow region. Due to the effect of mud on the wavelength inside the mud region, the wave crests in the lee of the region become discontinuous with those outside it; this effect is also seen in wave propagation over two-dimensional varying bathymetry (e.g., Berkhoff et al., 1982). Eventually, further downwave of the mud region. the bisected wave crests intersect, resulting in a hexagonal pattern similar to the intersecting cnoidal waves generated in the laboratory by Hammack et al. (1989).

In the classic case of wave diffraction around a detached breakwater, the extent of the shadow zone is strongly dependent on the width of the breakwater (Penney and Price, 1952). We anticipate that a similar dependence is evident on the longshore dimension of the mud patch. We decrease the longshore extent of the mud patch considerably (250 m $\leq y_{mud} \leq$ 350 m) and rerun the simulation. The result is shown in Fig. 9. Similar to the problem of a detached breakwater, the longshore extent of the shadow zone in the lee of the mud patch is closely related to that of the mud patch. In contrast to Fig. 8, here we see a much narrower shadow zone. Additionally, well into the lee, the intersection of the crests generate a wave traveling at the mean direction, a nonlinear effect similar to the hexagonal patterns seen in Fig. 8. From the point of view of using remote sensing to seed inverse models to infer the nature of the bottom, this sensitivity to patch size is encouraging provided there is sufficient damping of the waves by the bottom mud.

6. Summary

In this study we have outlined the development of a nonlinear wave model adapted with a mechanism for dissipation by a thin layer of viscous mud. The viscous damping mechanism used was formulated by Ng (2000) as a boundary-layer reduction of the model of Dalrymple and Liu (1978) for damping by a lower layer of viscous mud of arbitrary depth.

The dispersion relation (5) resulting from the theory of Ng (2000) is complex; the rate of viscous damping is contained in the imaginary part of the dispersion relation (6), while the effect of the mud on wave kinematics is contained in the real part (12). Ng (2000) detailed the damping effect of the theory but did not investigate the effect on the wavelength. We showed that the theory of Ng (2000) does decrease the wavenumber as $\tilde{d}$, the normalized mud depth, increases; however, the rate of this decrease is less than that shown by Dalrymple and Liu (1978). Thus, the viscous mud layer will not alter the detuning of the

nonlinear interactions (dependent on the wavenumbers of the interacting triads) relative to that with no mud present. The dependence of the damping rate (6) on the relative water depth kh is shown in Fig. 2; there is an apparent maximum damping near $kh \sim 0.88$, though the location of this maximum will change with different h and $\tilde{d}$.

The parabolic nonlinear model of Kaihatu and Kirby (1995) is used as the primary wave model for weakly nonlinear, fully dispersive waves, with the implementation of the viscous damping mechanism of Ng (2000) performed in a manner similar to the surf zone dissipation model of Kirby and Dalrymple (1986). The model was then tested against the experimental data of De Wit (1995) and shown to compare well, despite the thin layer assumption behind the dissipation mechanism.

Further testing was then performed in both one and two spatial dimensions, consisting of a permanent form cnoidal wave propagating over mud patches. Two general cases for mud viscosity were detailed. The first used a mud viscosity $v_m=1.3 \times 10^{-4}$ m²/s, or a viscosity ratio $\zeta=10$. The second used $v_m=1.3 \times 10^{-2}$ m²/s, or $\zeta=100$. For each case the density ratio $\gamma=(0.25,0.5,0.75,0.9)$. The mud depth d_m was selected for each viscosity case such that the dimensionless ratio $\tilde{d}=d_m/\delta_m=1$, where δ_m is the Stokes boundary layer thickness in the mud layer.

For the one-dimensional scenario, the cnoidal waveform retained its general shape for the $\zeta=10$ case, while for the highly-damped $\zeta=100$ case the waveform (to the extent that dissipation did not obscure it) appeared to be more sinusoidal. This indicates that there is some preferential dampening at the higher frequencies of the wavefield, in line with the kh-dependent dissipation shown in Fig. 2.

To elucidate this further, the amplitudes of the wavefield were plotted for the different γ values for each viscosity case (Fig. 6), both at the initial condition and at the downwave side of the mud patch. While the amplitudes for the $\zeta=10$ case monotonically decreased with frequency at the end of the mud patch, the $\zeta=100$ case did not, with the fourth harmonic of the wavefield exhibiting the greatest dissipation relative to the initial condition. For this harmonic $kh \sim 0.89$, which is close to the location of the dissipation maximum shown in Fig. 2.

It was also apparent that the frequencies beyond the deep water limit displayed some degree of attenuation over the mud patch for both viscosity cases, perhaps due to subharmonic interactions between them and lower, actively-dissipated frequencies. The one-dimensional model was run again for both $\zeta=10$ and $\zeta=100$ ($\gamma=0.9$). One run was performed with nonlinearity deactivated, and another with subharmonic interactions (first summation on right side of Eq. (17)) deactivated. It was shown (Fig. 7) that the amplitudes for both the linear and reduced nonlinear cases matched very closely and exhibited no reduction from the mud patch in the high frequencies. This indicates that the (deactivated) subharmonic interactions are responsible for the dissipation of the high frequencies of the wavefield, even if beyond the deep water limit. This is in line with the finding of Sheremet et al. (2005) for the case of wave groups.

The two-dimensional model was then applied to investigate wave propagation over a mud patch of limited longshore extent. Fig. 8 shows a result for a mud patch whose longshore dimension is half that of the domain. Very strong damping occurs inside the patch, leading to significant diffraction on the lee side. Further downwave, the discontinuity in the wave crest caused by the mud patch begins to resolve into a hexagonal wave pattern, as the two halves of the bisected wave crest rejoin. Limiting the longshore extent of the mud patch (Fig. 9) leads to a very different pattern on the downwave side. Since less of the wave crest experiences damping, there is less diffraction.

Future work with the model will involve surf zone dissipation and the resultant damping compared to that caused by mud. Of particular interest would be the alteration of the velocity moments required for nearshore sediment transport calculations. We also anticipate the opportunity to perform comparisons with field data.

Acknowledgments

References

Agnon, Y., Sheremet, A., 1997. Stochastic nonlinear shoaling of directional spectra. Journal of Fluid Mechanics 345, 79–99.

Agnon, Y., Sheremet, A., 2000. Stochastic evolution models for nonlinear gravity waves over uneven topography. In: Liu, P.L.-F. (Ed.), Advances in Coastal and Ocean Engineering, vol. 6. World Scientific.

Agnon, Y., Sheremet, A., Gonsalves, J., Stiassnie, M., 1993. Nonlinear evolution of a unidirectional shoaling wave field. Coastal Engineering 20, 29–58.

Ardhuin, F., Drake, T.G., Herbers, T.H.C., 2002. Observations of wave-generated vortex ripples on the North Carolina continental shelf. Journal of Geophysical Research 107. doi:10.1029/2001JC000986.

Ardhuin, F., O'Reilly, W.C., Herbers, Th.C., Jessen, P.F., 2003. Swell transformation across the continental shelf. Part 1: attenuation and swell broadening. Journal of Physical Oceanography 33, 1921–1939.

Berkhoff, J.C.W., 1972. Computation of combined refraction–diffraction. 13th International Conference on Coastal Engineering. ASCE, Vancouver, BC, pp. 471–490.

Berkhoff, J.C.W., Booij, N., Radder, A.C., 1982. Verification of numerical wave propagation models for simple harmonic linear waves. Coastal Engineering 6, 255–279.

Booij, N., Ris, R.C., Holthuijsen, L.H., 1999. A third generation wave model for coastal regions. 1. Model description and validation. Journal of Geophysical Research 104, 7649–7666.

Chou, H.T., Foda, M.A., Hunt, J.R., 1993. Rheological response of cohesive sediments to oscillatory forcing. In: Mehta, A.J. (Ed.), Nearshore and

Estuarine Cohesive Sediment Transport. Coastal and Estuarine Sciences, vol. 42. AGU, pp. 126–148.

Dalrymple, R.A., Liu, P.L.F., 1978. Waves over soft muds: a two-layer fluid model. Journal of Physical Oceanography 8, 1121–1131.

De Wit, P.J., 1995. Liquifaction of cohesive sediment by waves. Ph.D. dissertation, Delft University of Technology.

Dean, R.G., Dalrymple, R.A., 1991. Water Wave Mechanics for Engineers and Scientists, Advanced Series on Ocean Engineering. World Scientific, Singapore.

Elgar, S., Guza, R.T., 1985. Observations of bispectra of shoaling surface gravity waves. Journal of Fluid Mechanics 161, 425–448.

Foda, M.A., 1989. Sideband damping of water waves over a soft bed. Journal of Fluid Mechanics 201, 189–201.

Foda, M.A., Hunt, J.R., Chou, H.T., 1993. A nonlinear model for the fluidization of marine mud by waves. Journal of Geophysical Research 98, 7039–7047.

Forristall, G.Z., Reece, A.M., 1985. Measurements of wave attenuation due to a soft bottom: SWAMP experiment. Journal of Geophysical Research 90, 3367–3380.

Freilich, M.H., Guza, R.T., 1984. Nonlinear effects on shoaling surface gravity waves. Philosophical Transactions of the Royal Society of London A 311, 1–41.

Gade, H.G., 1958. Effects of a nonrigid, impermeable bottom on place waves in shallow water. Journal of Marine Research 16, 61–82.

Hammack, J., Scheffner, N., Segur, H., 1989. Two-dimensional periodic waves in shallow water. Journal of Fluid Mechanics 209, 567–589.

Herbers, T.H.C., Burton, M.C., 1997. Nonlinear shoaling of directionally spread waves on a beach. Journal of Geophysical Research 102, 21101–21114.

Hill, D.F., Foda, M.A., 1998. Subharmonic resonance of oblique interfacial waves by a progressive surface wave. Proceedings, Royal Society of London A 454, 1129–1144.

Hsiao, S.V., Shemdin, O.H., 1980. Interaction of ocean waves with a soft bottom. Journal of Physical Oceanography 10, 605–610.

Jamali, M., Lawrence, G.A., Seymour, B., 2003. A note on the resonant interaction between a surface wave and two interfacial waves. Journal of Fluid Mechanics 491, 1–9.

Jaramillo, S., Sheremet, A., Allison, M.A., Dartez, S., 2006. Coupled evolution of waves and fluid mud layers. Poster presented at American Geophysical Union Ocean Sciences Meeting, Honolulu, HI.

Jiang, F., Mehta, A.J., 1995. Mudbanks of the southwest coast of India IV: mud viscoelastic properties. Journal of Coastal Research 11, 918–926.

Jiang, F., Mehta, A.J., 1996. Mudbanks of the southwest coast of India V: wave attenuation. Journal of Coastal Research 12, 890–897.

Jiang, L., Zhao, Z., 1989. Viscous damping of solitary waves over fluid–mud seabeds. Journal of Waterway, Port, Coastal and Ocean Engineering (ASCE) 115, 345–362.

Jiang, L., Kioka, W., Ishida, A., 1990. Viscous damping of cnoidal waves over fluid–mud seabed. Journal of Waterway, Port, Coastal and Ocean Engineering (ASCE) 116, 470–491.

Kaihatu, J.M., 2001. Improvement of parabolic nonlinear dispersive wave model. Journal of Waterway, Port, Coastal and Ocean Engineering (ASCE) 127, 113–121.

Kaihatu, J.M., Kirby, J.T., 1995. Nonlinear transformation of waves in finite water depth. Physics of Fluids 7, 1903–1914.

Kirby, J.T., Dalrymple, R.A., 1986. Modeling waves in surf zones and around islands. Journal of Waterway, Port, Coastal and Ocean Engineering (ASCE) 112, 78–93.

Kirby, J.T., Kaihatu, J.M., 1996. Structure of frequency domain models for random wave breaking. In: Edge, B.L. (Ed.), 25th International Conference on Coastal Engineering. ASCE, Orlando, FL, pp. 1144–1155.

Lee, S.C. 1995. Response of mud profiles to waves. Ph.D. dissertation, Department of Civil and Coastal Engineering, University of Florida, Gainesville, FL.

Liu, P.L.F., Yoon, S.B., Kirby, J.T., 1985. Nonlinear refraction–diffraction of waves in shallow water. Journal of Fluid Mechanics 153, 184–201.

Macpherson, H., 1980. The attenuation of water waves over a non-rigid bed. Journal of Fluid Mechanics 97, 721–742.

Mathew, J. (1992). Wave-mud interaction in mud banks. Ph.D. dissertation, Cochin University of Schience and Technology, Cochin, India.

Mehta, A.J., Srinivas, R., 1993. Observations of entrainment of fluid mud by shear flow. In: Mehta, A.J. (Ed.), Nearshore and Estuarine Cohesive Sediment Transport. American Geophysical Union, Washington DC, pp. 224–246.

Mei, C.C., Liu, K.F., 1987. A Bingham-plastic model for a muddy seabed under long waves. Journal of Geophysical Research 92, 14581–14594.

Ng, C.O., 2000. Water waves over a muddy bed: a two-layer Stokes' boundary layer model. Coastal Engineering 40, 221–242.

Penney, W.G., Price, A.T., 1952. The diffraction of sea waves and the shelter afforded by breakwaters. Philosophical Transactions of the Royal Society of London. Series A 244, 236–253.

Peregrine, D.H., 1967. Long waves on a beach. Journal of Fluid Mechanics 27, 815–827.

Radder, A.C., 1979. On the parabolic equation method for water wave propagation. Journal of Fluid Mechanics, 95, 159–176.

Sheremet, A., Stone, G.W., 2003. Observations of nearshore wave dissipation over muddy sea beds. Journal of Geophysical Research 108, 3357–3368.

Sheremet, A., Mehta, A.J., Kaihatu, J.M., 2005. Wave–sediment interaction on a muddy shelf. Proceedings, Fifth International Symposium on Ocean Wave Measurement and Analysis, Madrid, Spain, to appear.

Tubman, M.W., Suhayda, J.N., 1976. Wave action and bottom movements in fine sediments. Proceedings, 15th International Conference on Coastal Engineering, Honolulu, HI, pp. 1168–1183.

Wells, J.T., Coleman, J.M., 1981. Physical processes and fine-grained seiment dynamics, coast of Surinam, South America. Journal of Sedimentary Petrology 15, 1053–1068.

Whitham, G.B., 1974. Linear and nonlinear waves. Wiley-Interscience, New York.

Winterwerp, J.C., de Graff, R.F., Groeneweg, J., Luijendijk, A.P., 2007. Modeling of wave damping at Guyana mud coast. Coastal Engineering 54, 249–261.

Yamamoto, T., Takahashi, S., 1985. Wave damping by soil motion. Journal of Waterway, Port, Coastal and Ocean Engineering (ASCE) 111, 62–77.

Yamamoto, T., Koning, H.L., Sellmeiher, H., van Hijum, E.V., 1978. On the response of a poro-elastic bed to water waves. Journal of Fluid Mechanics 87, 193–206.

REPORT DOCUMENTATION PAGE

Form Approved
OMB No. 0704-0188

The public reporting burden for this collection of information is estimated to average 1 hour per response, including the time for reviewing instructions, searching existing data sources, gathering and maintaining the data needed, and completing and reviewing the collection of information. Send comments regarding this burden estimate or any other aspect of this collection of information, including suggestions for reducing the burden, to the Department of Defense, Executive Services and Communications Directorate (0704-0188). Respondents should be aware that notwithstanding any other provision of law, no person shall be subject to any penalty for failing to comply with a collection of information if it does not display a currently valid OMB control number.
PLEASE DO NOT RETURN YOUR FORM TO THE ABOVE ORGANIZATION.

1. REPORT DATE (DD-MM-YYYY)	2. REPORT TYPE	3. DATES COVERED (From - To)
04-06-2008	Journal Article	

4. TITLE AND SUBTITLE	5a. CONTRACT NUMBER
A Model for the Propagation of Nonlinear Surface Waves Over Viscous Muds	
	5b. GRANT NUMBER
	5c. PROGRAM ELEMENT NUMBER
	0601153N

6. AUTHOR(S)	5d. PROJECT NUMBER
James M. Kaihatu, Alexandru Sheremet, K. Todd Holland	
	5e. TASK NUMBER
	5f. WORK UNIT NUMBER
	73-8580-06-5

7. PERFORMING ORGANIZATION NAME(S) AND ADDRESS(ES)	8. PERFORMING ORGANIZATION REPORT NUMBER
Naval Research Laboratory Oceanography Division Stennis Space Center, MS 39529-5004	NRL/JA/7320-06-6266

9. SPONSORING/MONITORING AGENCY NAME(S) AND ADDRESS(ES)	10. SPONSOR/MONITOR'S ACRONYM(S)
Office of Naval Research 800 N. Quincy St. Arlington, VA 22217-5660	ONR
	11. SPONSOR/MONITOR'S REPORT NUMBER(S)

12. DISTRIBUTION/AVAILABILITY STATEMENT

Approved for public release, distribution is unlimited.

13. SUPPLEMENTARY NOTES

14. ABSTRACT

The effect of a thin viscous fluid-mud layer on nearshore nonlinear wave-wave interactions is studied using a parabolic frequency-domain nonlinear wave model, modified to incorporate a bottom dissipation mechanism based on a viscous boundary layer approach. The boundary-layer formulation allows for explicit calculation of the mud-induced wave damping rate. The model performed well in tests based on laboratory data. Numerical tests show that damping of high frequency waves occurs, mediated by "difference" nonlinear interactions. Simulations of 2-dimensional wave propagation over a mud "patch" of finite extent show that the wave dissipation causes significant downwave diffraction effects.

15. SUBJECT TERMS

viscous muds, Boussinesq, propagation

16. SECURITY CLASSIFICATION OF:			17. LIMITATION OF ABSTRACT	18. NUMBER OF PAGES	19a. NAME OF RESPONSIBLE PERSON
a. REPORT	b. ABSTRACT	c. THIS PAGE			James Kaihatu
Unclassified	Unclassified	Unclassified	UL	13	19b. TELEPHONE NUMBER (Include area code) 228-688-5710

Standard Form 298 (Rev. 8/98)
Prescribed by ANSI Std. Z39.18